Crystal Structures of Constitutive Nitric Oxide Synthases in Complex with De Novo Designed Inhibitors†

Jotaro Igarashi,‡,|| Huiying Li,‡ Joumana Jamal,‡ Haitao Ji,§ Jianguo Fang,§ Graham R. Lawton,§ Richard B. Silverman,§ and Thomas L. Poulos*,‡

Departments of Molecular Biology and Biochemistry, Pharmaceutical Sciences, and Chemistry, University of California, Irvine, California 92697-3900, Department of Chemistry, Department of Biochemistry, Molecular Biology, and Cell Biology, Center for Drug Discovery and Chemical Biology, Northwestern University, Evanston, Illinois 60208-3113

Received January 6, 2009

New nitric oxide synthase (NOS) inhibitors were designed de novo with knowledge gathered from the studies on the nNOS-selective dipeptide inhibitors. Each of the new inhibitors consists of three fragments: an aminopyridine ring, a pyrrolidine, and a tail of various length and polarity. The in vitro inhibitory assays indicate good potency and isoform selectivity for some of the compounds. Crystal structures of these inhibitors bound to either wild type or mutant nNOS and eNOS have confirmed design expectations. The aminopyridine ring mimics the guanidinium group of L-arginine and functions as an anchor to place the compound in the NOS active site where it hydrogen bonds to a conserved Glu. The rigidity of the pyrrolidine ring places the pyrrolidine ring nitrogen between the same conserved Glu and the selective residue nNOS Asp597/eNOS Asn368, which results in similar interactions observed with the α-amino group of dipeptide inhibitors bound to nNOS. These structures provide additional information to help in the design of inhibitors with greater potency, physicochemical properties, and isoform selectivity.

Introduction

Three different mammalian isoforms of nitric oxide synthase (NOS[a]) have been isolated and characterized: neuronal (nNOS), inducible (iNOS), and endothelial (eNOS). Although different isoforms have different cell and tissue distribution and are regulated through various mechanisms, they all catalyze the conversion of one guanidinium N atom of L-arginine (L-Arg) to nitric oxide. All three isoforms share a similar domain architecture with a N-terminal domain consisting of the catalytic heme active site and a cofactor, tetrahydrobiopterin, binding site, while the C-terminal domain containing FMN, FAD, and NADPH binding sites serves as an electron donating domain.[1,2] The linker between the two functional domains is a calmodulin binding motif. The binding of calmodulin enables electron flow from the flavins to the heme.[3]

Nitric oxide is an important signaling molecule involved in a wide range of physiological functions in the neuronal, immune, and cardiovascular system.[4,5] To exert appropriate functions, NO generation by the three different NOS isoforms is under tight regulation. The overproduction of NO by nNOS (or iNOS) and the underproduction by eNOS have been shown to lead to pathophysiological conditions such as neurodegenerative diseases,[6] stroke,[7,8] rheumatoid arthritis,[9] hypertension,[10] and atherosclerosis.[11] Inhibition of nNOS (or iNOS) can thus be of considerable therapeutic benefit. However, inhibition must be isoform selective so that only NO formation by the disease-associated NOS, (e.g., nNOS) will be inhibited by the treatment, while the physiological function of the other isoform, often eNOS, is unaffected. Isoform-selective inhibition is a challenging problem given that the three isoforms have very few differences in their three-dimensional structures.

Previous structure−activity studies in our laboratories on a series of N^{ω}-nitro-L-arginine containing dipeptide inhibitors[12,13] (Figure 1A) have uncovered some key structural features in the NOS active site that are responsible for the selective binding affinity of these inhibitors to nNOS over eNOS.[14−17] Most importantly, the single amino acid difference, Asp597 in nNOS and Asn368 in eNOS, had been identified as the major reason why inhibitors **1**, **2**, and **3** (Figure 1A) bind more tightly to nNOS than eNOS. In nNOS, these inhibitors adopt a curled binding mode that places the inhibitor α-amino group between Asp597 and Glu592 for optimal electrostatic stabilization. Because eNOS has Asn368 rather than Asp, there is no energetic incentive for the inhibitor to curl, and instead the inhibitors adopt an extended conformation. One obvious design principle to emerge from this work is to have a positively charged group corresponding to the α-amino group in **1**, **2**, or **3** on a rigid scaffold such that the inhibitor will not have to curl in order to optimize charge interactions with Asp597 and Glu592. One other design principle is to replace the nitro-guanidinium group with an aminopyridine primarily because the aminopyridine should mimic the H-bonding pattern of the nitro-guanidinium, while the pK_a of the aminopyridine group (≈6−7) should increase bioavailability.[18,19] On the basis of these design principles, a new de novo design method was proposed and a series of new inhibitors, **4**, **5**, **6**, and **7** (Figure 1B), have been synthesized, the in vitro inhibitory potency determined, and the inhibitors applied to an animal model.[18,19] Here we report the crystal

† Crystallographic coordinates have been deposited with the Protein Data Base with accession codes 3B3M, 3B3N, 3B3O, 3B3P, 3DQR, 3DQS, and 3DQT.

* To whom correspondence should be addressed. Phone: 949-824-7020. Fax: 949-824-328. E-mail: poulos@uci.edu.

‡ Departments of Molecular Biology and Biochemistry, Pharmaceutical Sciences, and Chemistry, University of California, Irvine.

§ Department of Chemistry, Department of Biochemistry, Molecular Biology, and Cell Biology, Center for Drug Discovery and Chemical Biology, Northwestern University.

|| Present address: Institute of Multidisciplinary Research for Advanced Materials, Tohoku University2-1-1 Katahira, Aoba-ku, Sendai 980-8577, Japan.

[a] Abbreviations used: NOS, nitric oxide synthase; nNOS, neuronal NOS; iNOS, inducible NOS; eNOS, endothelial NOS; 2′,5′-ADP, adenosine 2′,5′-diphosphate; CCD, charge coupled device; MM-PBSA: molecular mechanics with Poisson−Boltzmann surface area methodology; GAFF: general Amber force field; AM1-BCC: Austin model 1-bond charge correction.

10.1021/jm900007a CCC: $40.75
Published on Web 03/18/2009

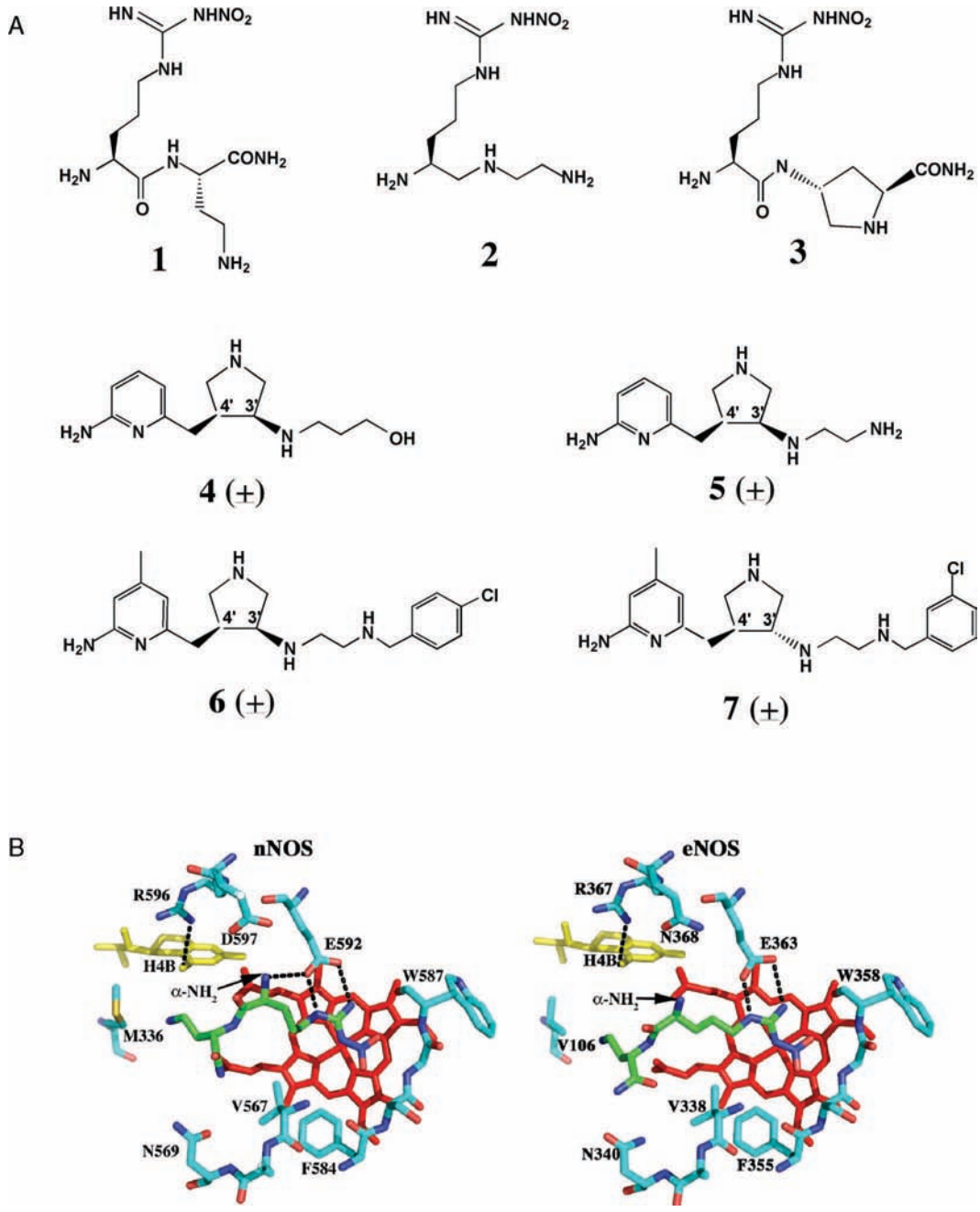

Figure 1. (A) Chemical structures and nomenclature for the inhibitors discussed in the paper. (**1**) L-N^{ω}-nitroarginine-2,4-L-diaminobutyramide; (**2**) (4*S*)-*N*-(4-amino-5-[aminoethyl]aminopentyl)-*N*″-nitroguanidine; (**3**) L-N^{ω}-nitroarginine-(4*R*)-amino-L-proline amide; (**4**) (±)-3-{*cis*-4′-[(6″-aminopyridin-2″-yl)methyl]pyrrolidin-3′-ylamino}propan-1-ol; (**5**) (±)-N^1-{*cis*-4′-[(6″-aminopyridin-2″-yl)methyl]pyrrolidin-3′-yl}ethane-1,2-diamine; (**6**) (±)-N^1-{*cis*-4′-[(6″-amino-4″-methylpyridin-2″-yl)methyl]pyrrolidin-3′-yl}-N^2-(4′-chlorobenzyl)ethane-1,2-diamine; (**7**) (±)-N^1-{*trans*-4′-[(6″-amino-4″-methylpyridin-2″-yl)methyl]pyrrolidin-3′-yl}-N^2-(3′-chlorobenzyl)ethane-1,2-diamine. (B) Structure of **1** complexed to nNOS and eNOS.[12] In nNOS, the inhibitor adopts a curled conformation in order to enable the inhibitor α-amino group to optimally interact with both Glu592 and Asp597. In eNOS, the residue corresponding to Asp597 is Asn368 and, as a result, the inhibitor adopts an extended conformation.

structures of these inhibitors bound to both eNOS and nNOS. Unfortunately, we were unable to obtain suitable crystals of eNOS in complex with **4** or **5**, which often is the case for inhibitors that bind poorly to eNOS.

Results

Binding of 4 and 5 to nNOS. Although all the new inhibitors **4** through **7** (Figure 1A) used for crystallographic studies are the racemic mixture, the electron densities of all four inhibitor complex structures show that only one enantiomer in each case is bound in the NOS active site. As expected, the two nitrogen atoms of the aminopyridine moiety of both **4** and **5** are involved in H-bonding with the Glu592 carboxylate (Figure 2), similar to the bifurcated H-bonding found between two guanidino nitrogens of dipeptide inhibitor and the Glu592 side chain oxygens in the nNOS dipeptide complex structures.[12] The pyridine ring is roughly parallel to and stacking against the heme plane with the closest distance from the C3 atom of pyridine to the NB atom of heme in the range of 3.3−3.4 Å. The rigid pyrrolidine ring indeed brings its nitrogen within H-bonding distance to the Glu592 side chain resembling the curled binding conformation of dipeptide inhibitor where the α-amino group forms a H-bond to Glu592. There are two hydrogen atoms attached to this nitrogen atom. One forms a H-bond with

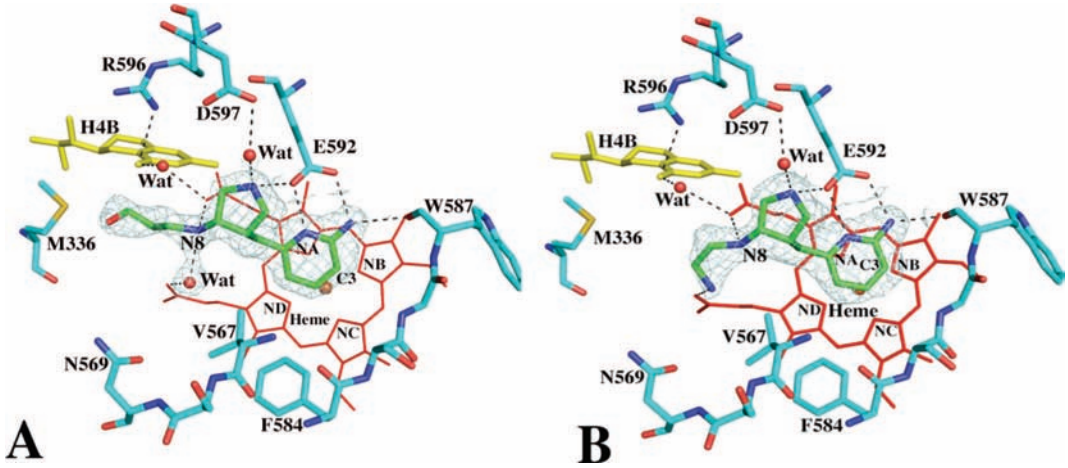

Figure 2. Active site structures of the wild type nNOS with inhibitor **4** (A) or **5** (B) bound viewed side by side in an identical orientation. Shown also the $F_o - F_c$ omit map contoured at 3.0σ for each inhibitor. Hydrogen bonds are drawn with the dashed lines. The atomic color scheme for amino acids is: carbon, cyan or green; nitrogen, blue; oxygen, red; sulfur, yellow. The figures are made with PyMol (http://pymol.sourceforge.net).

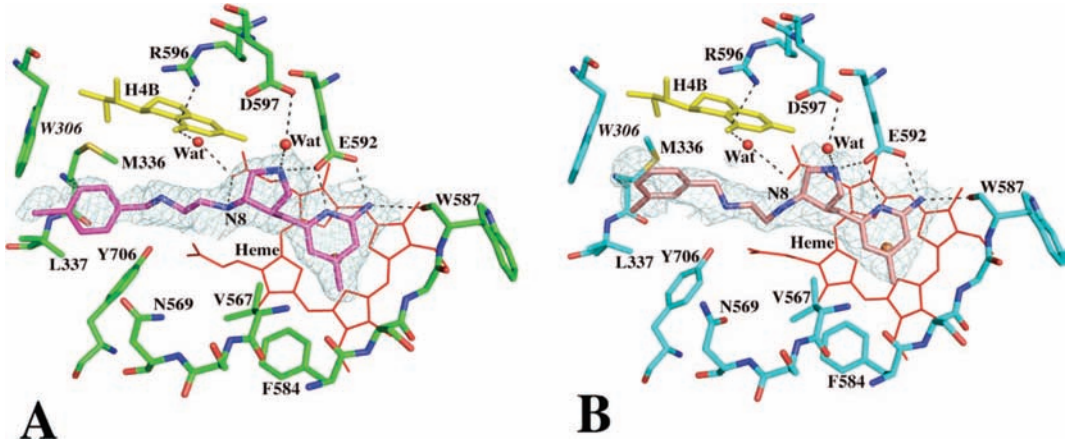

Figure 3. Active site structures of the wild type nNOS with inhibitor **6** (A) or **7** (B) bound. Density around each inhibitor is the $F_o - F_c$ omit map contoured at 3.0σ. Residue Trp306 belongs to the neighboring subunit.

Glu592. Another one forms a H-bond with a conserved structural water, which then forms H-bond interactions with Asp597. The amino group next to the pyrrolidine ring (N8 in Figure 2), mimicking the peptide amide nitrogen in the dipeptide inhibitor, makes a direct H-bond with the heme propionate group of pyrrole ring A. The tails of compounds **4** and **5** adopt quite different conformations. The amino group of **5** curls back to make a H-bond to the second heme propionate, while the hydroxyl group of **4**, owing to its one carbon longer arm, can no longer make any direct contact with the heme (Figure 2). This additional charge−charge interaction between the terminal amine of **5** and heme propionate is probably a major factor contributing to the tighter binding of inhibitor **5** (K_i = 0.388 μM) compared to **4** (K_i = 9.4 μM).

Binding of 6 and 7 to nNOS. Inhibitors **6** and **7** were derived from **5** with two modifications (Figure 1A). First, a methyl group was introduced in the aminopyridine ring to provide additional contacts with a small hydrophobic pocket surrounded by Val567 and Phe584. Second, a chlorobenzyl group was attached to the terminal amino position in order to reach into a region where different NOS isoforms start to show sequence diversity. Inhibitor **6**, similar to **4** and **5**, has a (3′*S*, 4′*S*) *cis*-conformation at the two chiral carbons on the pyrrolidine ring. Its aminopyridine and pyrrolidine rings, therefore, bind to the active site the same as **4** and **5**, as described previously[19] (Figure 3A). Inhibitor **7**, on the other hand, possesses a (3′*R*,4′*S*)*trans*-conformation. However, the H-bonding interactions from both its aminopyridine and pyrrolidine rings to the Glu592 side chain are still retained (Figure 3B). The newly added methyl group in both **6** and **7** makes van der Waals contact with Phe384 with a closest distance of 3.6 Å. Larger differences between **6** and **7** are seen in the third fragment beyond the pyrrolidine ring. The 3′*S* conformation in the pyrrolidine of **6** places the neighboring amino group (N8 in Figure 3) downward toward the heme where it H-bonds with the heme propionate (Figure 3A), whereas the 3′*R* conformation in **7** brings N8 away from the propionate (Figure 3B). Lack of this H-bond in **7** might be one of the reasons **7** (K_i = 0.25 μM) binds more poorly to nNOS than does **6** (K_i = 0.085 μM). The remaining chain leads the chlorophenyl moiety to a hydrophobic pocket defined by Met336, Leu337, Tyr706, and Trp306 of the neighboring subunit. However, the exact orientation of the chlorophenyl ring is somewhat ambiguous owing to the poor density quality in the region, especially in the structure of the **7** complex.

Binding of 6 and 7 to eNOS. As expected, inhibitors **6** and **7** bind very much the same to eNOS (Figure 4). Part of the inhibitor design effort was to rigidify the inhibitor such that the key amino group interacting with Asp597 in nNOS would

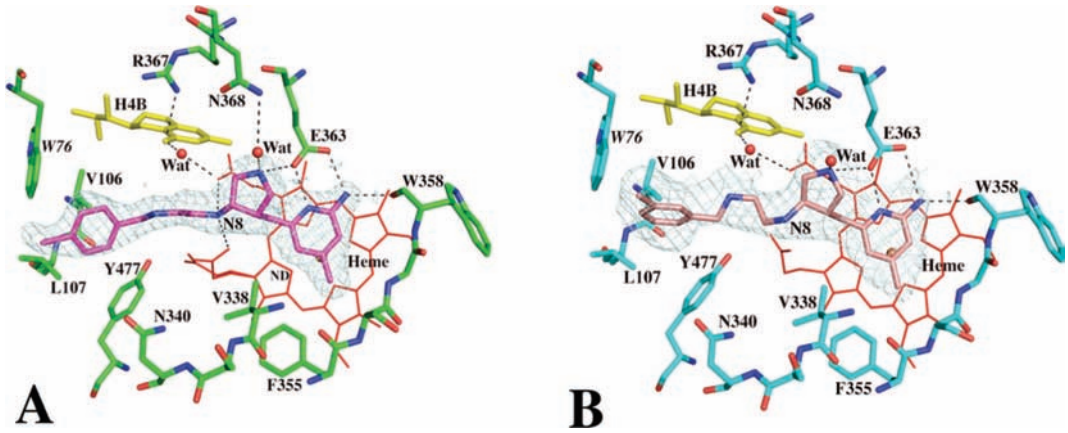

Figure 4. Active site structures of the wild type eNOS with inhibitor **6** (A) or **7** (B) bound. Also shown around the inhibitor is the $F_o - F_c$ omit map contoured at 3.0σ. Residue Trp76 belongs to the neighboring subunit. Alternate conformations of heme propionate off the pyrrole ring D are also depicted.

bind the same in eNOS.[18,19] This is exactly what happens. The pyrrolidine N atom is positioned the same in both eNOS and nNOS even to the extent that in both NOS isoforms a water molecule bridges between the pyrrolidine N atom and Asp597 in nNOS (Asn368 in eNOS). However, the pyrrolidine N atom should experience greater electrostatic stabilization in nNOS because nNOS has two negative charges nearby, Asp597 and Glu592, while eNOS has only Glu363. A second difference involves the chlorophenyl tail. In nNOS, the aromatic ring can potentially form closer contacts with Met336 compared to the smaller corresponding residue, Val106, in eNOS. However, the electron density for the chlorophenyl group is more well-ordered in eNOS than in nNOS and thus it is doubtful that differences in interaction between the inhibitor aromatic ring and protein is a major contributor to isoform selectivity. The primary source of the 1000-fold selectivity is more likely due to the greater electrostatic stabilization to the pyrrolidine N atom of **6** in nNOS.

Inhibitor Binding to the nNOS Asp597Asn/Met336Val Mutant. In previous work, we converted Asp597 and Met336 in nNOS to the corresponding residues in eNOS, Asn, and Val, in order to test our hypothesis that both of these residues form more favorable contacts with the dipeptide inhibitors in nNOS than in eNOS.[13] Consistent with the finding that the binding mode of the new inhibitors reported here is unchanged between nNOS and eNOS, they also maintain the identical binding mode when wild type and mutant nNOS structures are compared. Inhibitor **5** found in the nNOS Asp597Asn/Met336Val double mutant structure has its aminopyridine and pyrrolidine rings H-bonded to Glu592 in a manner similar to that observed in wild type nNOS (Figure 5). The only difference is that the terminal amino group in the mutant structure has weak density and seems not to form a H-bond with the heme propionate from pyrrole ring D in contrast to the case in the wild type nNOS−**5** complex structure. As expected, the K_i values for the nNOS double mutant increase for all inhibitors but the mutant still binds these inhibitors better than eNOS. Although we were not able to obtain suitable crystals of the eNOS−**5** complex, it is probably safe to assume that **5** forms a complex with eNOS very similar to the one observed in nNOS and the nNOS double mutant. What then needs to be explained is why wild type nNOS binds **5** about 1070-fold better than eNOS but only 90-fold better than the nNOS double mutant, a difference of 11-fold in K_i. In terms of free energy a factor of 11 accounts to $\approx$ 1.4 kcal/mol. It is possible that the tail primary amino group may be the source of this difference. In the wild type nNOS structure, the primary amino group of **5** has strong and continuous electron density with a heme propionate, but this is not the case in the nNOS double mutant. An even weaker interaction between this amino group and the heme propionate in eNOS could easily account for 1.4 kcal/mol.

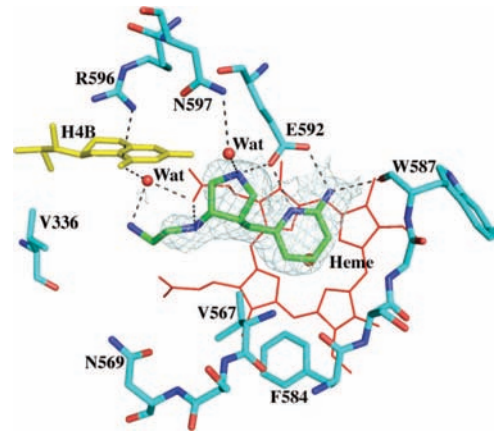

Figure 5. Active site structure of the nNOS Asp597Asn/Met336Val mutant with inhibitor **5** bound. The $F_o - F_c$ omit map is shown around the inhibitor contoured at 3.0σ.

MM-PBSA to Estimate ΔG of Binding. It would be advantageous to employ a rapid computational method to estimate which inhibitors not only bind best but exhibit greater selectivity for nNOS over eNOS. Toward this end, we have been using the MM-PBSA methodology as implemented in Amber 9.0 to compute ΔG_{bind}. The procedure described in Experimental Section was used to compute ΔG_{bind} for four different NOS inhibitors in five different crystal structures. As shown in Figure 6A, these are all aminopyridine inhibitors similar to inhibitors used for the crystal structures described in this study. However, because the K_i values from which ΔG_{exp} are derived for inhibitors **4**, **5**, **6**, and **7** used in the present study are mixtures of optical isomers, these were not included in the training set for generating Figure 6B. Figure 6B is a plot of computed free energy obtained from single energy minimized structures[20,21] vs experimental free energies derived from K_i measurements. The computed free energies are much larger because we have not included inhibitor entropy corrections. Even so, the fit is quite good. Although the inhibitors used in Figure 6 are very similar, they span a K_i range of over 10^3, yet the relative ΔG_{calc} agrees well with ΔG_{exp}.

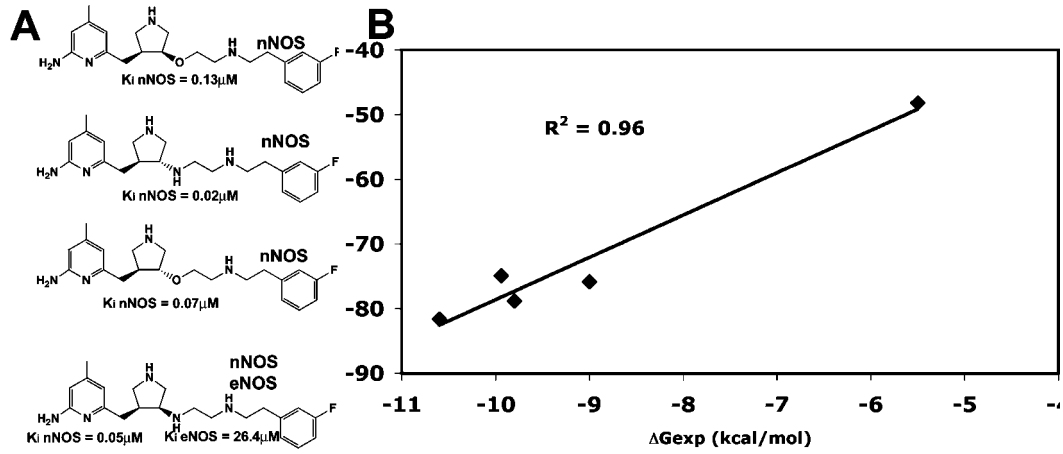

Figure 6. (A) Structures of the various inhibitors complexed with either eNOS, nNOS, or both used to construct the plot in panel B. (B) Plot of experimental ΔG_{exp} vs computed ΔG_{calc} using five different crystal structures.

Table 1. In Vitro NOS Inhibition (K_i in μM)

inhibitor	nNOS	eNOS	nNOS DM	eNOS/nNOS	$\Delta\Delta G_{exp}$ (kcal/mol)	$\Delta\Delta G_{calc}$ (kcal/mol)
1	0.3	107.0		357		
2	0.15	80.0		533		
3	0.10	110.0		1100		
4 (±)	9.4	366.6	49.2	39	2.2	1.3
5 (±)	0.388	416.7	36.7	1068	4.2	4.1
6 (±)	0.085	85.2	1.2	1002		
7 (±)	0.25	95.2	6.1	381		

Inhibitors **4** and **5** were used with the plot in Figure 6B as test cases. Because we do not have crystal structures of these inhibitors bound to eNOS, **4** and **5** were modeled into the eNOS active site pocket by assuming that they adopt the same binding mode as in nNOS. ΔG_{calc} was calculated using the protocol outlined in the Experimental Section and converted to the same scale as experimental, ΔG_{exp}, using the straight line equation derived from Figure 6B.

$$\Delta G_{calc}(\text{corrected}) = (\Delta G_{calc} + 12.12)/6.55$$

$\Delta\Delta G$ is defined as the difference in binding free energy between nNOS and eNOS, $\Delta\Delta G = \Delta G_{bind}(\text{nNOS}) - \Delta G_{bind}(\text{eNOS})$. For inhibitor **4**, $\Delta\Delta G_{exp} = 2.2$ kcal/mol and $\Delta\Delta G_{calc} = 1.3$ kcal/mol, while for **5**, $\Delta\Delta G_{exp} = 4.2$ kcal/mol and $\Delta\Delta G_{calc} = 4.1$ kcal/mol (Table 1). It thus appears that the simplified MM-PBSA method used here is capable of correctly estimating NOS isoform selectivity and should prove useful in prescreening novel NOS inhibitors of similar structure.

Discussion

The present work illustrates that fairly simple design principles derived from our previous work[12,22] can be used to prepare novel NOS inhibitors that retain isoform selectivity but might exhibit improved pharmacological properties. As in the earlier dipeptide inhibitor work, the key to isoform selectivity is the Asp597 (nNOS) vs Asn368 (eNOS) difference. The pyrrolidine ring N atom and its close proximity to two negative charges in the nNOS active site compared to only one negative charge in the eNOS active site appears to be the key factor controlling selectivity. The advantage of these newer pyrrolidine inhibitors is that they are fairly rigid compared to the dipeptide inhibitors used in our previous work and all bind the same to eNOS and nNOS; therefore, understanding the structural basis for selectivity is not complicated by differences in inhibitor conformation as in the case of the dipeptide inhibitors. The simplified MM-PBSA procedure, where only a single energy minimized structure is used and entropic factors ignored, does a reasonably good job in estimating isoform selectivity and is very rapid.

The ultimate practical outcome of these efforts is to develop therapeutic agents that can treat neuropathological conditions associated with the overproduction of NO by nNOS. Very recently, our groups have shown that compounds closely related to **6** are capable of significant protection against neural damage in a rabbit cerebral palsy model.[19] Moreover, protection is associated with a decrease in brain NO production and brain NOS activity without affecting eNOS regulated blood pressure. Our efforts on NOS structure-based drug design thus add to a short but growing documented list where the close interaction between structural biology, medicinal chemistry, and computer modeling can result in the development of novel compounds with demonstrated in vivo therapeutic effects.

Experimental Section

Protein and Crystal Preparations. The full-length, wild type or mutant, nNOS and eNOS proteins were expressed in *E. coli* strain BL21 (DE3). The proteins were purified with Ni Sepharose and/or 2′,5′-ADP Sepharose columns as described previously.[12,13,23] The heme domain nNOS or eNOS was generated from the partially purified full-length enzymes by limited trypsin digest. The heme domain protein was further separated from the fragments of the reductase domain by gel filtration through a Superdex 200 column.[23]

The purified nNOS or eNOS heme domain protein was concentrated to 7−9 (nNOS) or 20 (eNOS) mg/mL. About 8−10 mM of inhibitor was added to the protein before the sitting drop vapor diffusion crystallization setups using the reservoir solutions reported earlier.[12,13,23] Crystallization plates were left in a 5 °C incubator for more than 2 days to allow crystals to reach full size. Fresh crystals of less than 10 days old were flash-cooled with liquid nitrogen after passing through a series of cyroprotectant solutions as described previously.[12,13,23]

Inhibitory Assays. Nitric oxide formation was monitored by the hemoglobin capture assay[24] with buffer components described previously.[25] The apparent K_i values were obtained by measuring percent inhibition in the presence of 10 μM L-arginine with various amount of inhibitor. The parameters of the following inhibition equation were fitted to the initial 1 min velocity data: % inhibition $= 100[I]/\{[I] + K_i(1 + [S]/K_m)\}$. K_m value for nNOS double mutant was determined to be 1.9 μM.

X-ray Diffraction Data Collection and Crystal Structure Determination. The X-ray diffraction data were collected under a liquid nitrogen stream (100 K) with CCD detectors either at Stanford Synchrotron Radiation Lightsource (SSRL, Menlo Park, CA) or at

Table 2. Data Collection and Refinement Statistics

data set[a]	nNOS **4**	nNOS **5**	nNOS **6**	nNOS **7**	nNOS DM **5**	eNOS **6**	eNOS **7**
PDB code	3B3M	3B3N	3B3O	3B3P	3DQR	3DQS	3DQT
cell dimensions(Å) (SG: $P2_12_12_1$)	$a = 51.50$	$a = 52.05$	$a = 52.21$	$a = 52.58$	$a = 51.87$	$a = 57.96$	$a = 58.25$
	$b = 109.53$	$b = 110.69$	$b = 111.53$	$b = 110.25$	$b = 110.70$	$b = 106.84$	$b = 106.49$
	$c = 163.25$	$c = 164.84$	$c = 164.84$	$c = 164.39$	$c = 164.36$	$c = 156.77$	$c = 156.42$
data resolution (Å)	1.95	1.98	2.05	2.45	2.40	2.03	2.54
total observations	279484	245363	217270	131153	155390	261113	140776
unique reflections	65107	66436	60556	35031	37670	64663	32771
R_{sym}[b]	0.040	0.064	0.052	0.101	0.094	0.054	0.089
	(0.251)[c]	(0.532)	(0.428)	(0.592)	(0.732)	(0.504)	(0.740)
$\langle I/\sigma \rangle$	15.9	11.7	10.7	6.3	7.2	9.6	9.2
	(5.1)[c]	(1.9)	(1.9)	(1.6)	(1.9)	(2.1)	(2.1)
completeness	94.9	98.7	97.8	98.7	99.3	99.9	99.6
(%)	(65.1)[c]	(90.1)	(96.1)	(99.4)	(99.0)	(100.0)	(99.9)
reflection used in refinement	64931	66359	60120	34892	37621	63716	32770
R factor[d]	0.204	0.230	0.213	0.209	0.205	0.197	0.197
R_{free}[e]	0.233	0.270	0.253	0.265	0.261	0.227	0.258
no. protein atoms	6663	6659	6677	6677	6819	6418	6439
no. heterogen atoms	165	163	181	181	163	209	199
no. water molecules	546	392	418	247	268	488	184
rms deviation							
bond length (Å)	0.007	0.009	0.010	0.009	0.010	0.009	0.010
bond angle (deg)	1.4	1.5	1.4	1.5	1.5	1.5	1.6

[a] nNOS DM refers to nNOS D597N/M336V double mutant. See Figure 1A for chemical structures and nomenclature of inhibitors. [b] $R_{sym} = \sum|I - \langle I \rangle|/\sum I$, where I is the observed intensity of a reflection and $\langle I \rangle$ the averaged intensity of multiple observations of the reflection and its symmetry mates. [c] The values in parentheses were obtained in the outermost resolution shell. [d] R factor $= \sum ||F_o| - |F_c||/\sum |F_o|$, F_o and F_c are the observed and calculated structure factors, respectively. [e] R_{free} was calculated with the 5% of reflections set aside randomly throughout the refinement.

Advanced Light Source (ALS, Berkeley, CA). Raw data were processed with HKL2000.[26] The binding of inhibitor was detected by difference Fourier synthesis. The inhibitor then was modeled into the density using O[27] and refined with CNS.[28] Water molecules were added automatically with CNS and inspected visually in O. The refined structures were validated before deposition to the RSCB data bank (http://deposit.pdb.org/validate/). The data collection and refinement statistics are summarized in Table 2.

Computational Approaches. The free energy of binding of various NOS inhibitors was estimated using the MM-PBSA method[29] as implemented in Amber 9.0. In this method, the total free energy of the NOS-inhibitor complex is taken as the sum of the following energy terms

$$G = E_{MM} + G_{solv} + G_{np} - TS_{solute}$$

where E_{MM} = the total molecular mechanics energy computed with the Sander module in Amber 9.0, G_{solv} is the solvation free energy estimated from the Poisson−Boltzmann equation, G_{np} = the nonpolar solvation energy estimated from the solvent accessible surface area, and TS_{solute} = the solute entropy. From a single energy minimized structure, the free energy was computed for the NOS−inhibitor complex, NOS alone with the inhibitor removed, and the inhibitor alone. The overall free energy of binding was computed from the following equation

$$\Delta G_{bind} = (G_{complex} - G_{receptor} - G_{inhibitor})$$

As others have done, the solute entropy was ignored.[30] Given that the inhibitors used for these calculations are structurally very similar with a similar number of rotatable bonds, ignoring inhibitor entropy introduces little error in comparing relative calculated and experimental free energies but does, of course, preclude the calculation of absolute free energies.

Inhibitor parameters and charges were assigned using the GAFF force field[31] and AM1-BCC charge scheme[32,33] as implemented in the Antechamber module in Amber 9.0. Heme parameters developed for cytochrome P450 were provided by Dr. Dan Harris.[34] It was necessary to carefully check the Antechamber output to make sure the correct atom types were assigned. For some inhibitors, it was necessary to increase the force constant on improper torsion angles from 1.1 to 10.1 kcal/Å in order to maintain planarity of the aminopyridine groups. To prepare the models for energetic calculations, all crystallographic waters were removed and TIP3 waters added back within 30 Å of the inhibitor. The resulting solvated structure was first energy minimized using the steepest descent method for 1000 cycles with the inhibitor and heme heavy atom restrained to the starting crystallographic positions. The restraints were relaxed to 10.0 kcal/Å^2 for the inhibitor and heme followed by another 1000 cycles of refinement. In the last step, the restraints for the heme and inhibitor were relaxed to 1.0 kcal/Å^2 followed by 1000 cycles of minimization. In the case of some eNOS−inhibitor complexes where structures were not determined but the nNOS−inhibitor complex structure was available, the inhibitor was positioned into the eNOS active site by assuming it adopts the same conformation and position as that found in nNOS.

Acknowledgment. This research was supported by NIH grants GM57353 (T.L.P.) and GM49725 (R.B.S.). We thank the beam line staff at SSRL and ALS for their assistance during data collections.

References

(1) Griffith, O. W.; Stuehr, D. J. Nitric oxide synthases: properties and catalytic mechanism. *Annu. Rev. Physiol.* **1995**, *57*, 707–736.
(2) Raman, C. S.; Martasek, P.; Masters, B. S. S. Structural themes determining function in nitric oxide synthases. In *The Porphyrin Handbook*, Kadish, K. M., Smith, K. M., Guilard, R., Eds.; Academic Press: San Diego, 2000; Vol. 4, pp 293−339.
(3) Abu-Soud, H. M.; Stuehr, D. J. Nitric oxide synthases reveal a role for calmodulin in controlling electron transfer. *Proc. Natl. Acad. Sci. U.S.A.* **1993**, *90*, 10769–10772.
(4) Moncada, S.; Palmer, R. M.; Higgs, E. A. Nitric oxide: physiology, pathophysiology, and pharmacology. *Pharmacol. Rev.* **1991**, *43*, 109–142.
(5) Kerwin, J. F., Jr.; Lancaster, J. R., Jr.; Feldman, P. L. Nitric oxide: a new paradigm for second messengers. *J. Med. Chem.* **1995**, *38*, 4343–4362.
(6) Dawson, V. L.; Dawson, T. M. Nitric oxide in neurodegeneration. *Prog. Brain Res.* **1998**, *118*, 215–229.
(7) Lipton, P. Ischemic cell death in brain neurons. *Physiol. Rev.* **1999**, *79*, 1431–1568.
(8) Sims, N. R.; Anderson, M. F. Mitochondrial contributions to tissue damage in stroke. *Neurochem. Int.* **2002**, *40*, 511–526.
(9) Bingham, C. O., III. The pathogenesis of rheumatoid arthritis: pivotal cytokines involved in bone degradation and inflammation. *J. Rheumatol., Suppl.* **2002**, *65*, 3−9.
(10) Taddei, S.; Virdis, A.; Ghiadoni, L.; Sudano, I.; Salvetti, A. Endothelial dysfunction in hypertension. *J. Cardiovasc. Pharmacol.* **2001**, *38* (Suppl. 2), S11–S14.

(11) Napoli, C.; de Nigris, F.; Williams-Ignarro, S.; Pignalosa, O.; Sica, V.; Ignarro, L. J. Nitric oxide and atherosclerosis: An update. *Nitric Oxide* **2006**, *15*, 265–279.

(12) Flinspach, M. L.; Li, H.; Jamal, J.; Yang, W.; Huang, H.; Hah, J. M.; Gomez-Vidal, J. A.; Litzinger, E. A.; Silverman, R. B.; Poulos, T. L. Structural basis for dipeptide amide isoform-selective inhibition of neuronal nitric oxide synthase. *Nat. Struct. Mol. Biol.* **2004**, *11*, 54–59.

(13) Li, H.; Flinspach, M. L.; Igarashi, J.; Jamal, J.; Yang, W.; Gomez-Vidal, J. A.; Litzinger, E. A.; Huang, H.; Erdal, E. P.; Silverman, R. B.; Poulos, T. L. Exploring the binding conformations of bulkier dipeptide amide inhibitors in constitutive nitric oxide synthases. *Biochemistry* **2005**, *44*, 15222–15229.

(14) Huang, H.; Martasek, P.; Roman, L. J.; Masters, B. S.; Silverman, R. B. *N*(omega)-Nitroarginine-containing dipeptide amides. Potent and highly selective inhibitors of neuronal nitric oxide synthase. *J. Med. Chem.* **1999**, *42*, 3147–3153.

(15) Huang, H.; Martasek, P.; Roman, L. J.; Silverman, R. B. Synthesis and evaluation of peptidomimetics as selective inhibitors and active site probes of nitric oxide synthases. *J. Med. Chem.* **2000**, *43*, 2938–2945.

(16) Hah, J. M.; Roman, L. J.; Martasek, P.; Silverman, R. B. Reduced amide bond peptidomimetics. (4*S*)-*N*-(4-amino-5-[aminoakyl]aminopentyl)-*N*′-nitroguanidines, potent and highly selective inhibitors of neuronal nitric oxide synthase. *J. Med. Chem.* **2001**, *44*, 2667–2670.

(17) Gomez-Vidal, J. A.; Martasek, P.; Roman, L. J.; Silverman, R. B. Potent and selective conformationally restricted neuronal nitric oxide synthase inhibitors. *J. Med. Chem.* **2004**, *47*, 703–710.

(18) Ji, H.; Stanton, B. Z.; Li, H.; Martásek, P.; Roman, L.; Poulos, T. L.; Silverman, R. B. Minimal pharmacophoric elements and a pharmacophore-driven strategy for fragment-based de novo design, an approach directed at molecular diversity and isozyme selectivity. design of selective neuronal nitric oxide synthase inhibitors. *J. Am. Chem. Soc.* **2008**, *130*, 3900–3914.

(19) Ji, H.; Tan, S.; Igarashi, J.; Li, H.; Derrick, M.; Martasek, P.; Roman, L. J.; Vasquez-Vivar, J.; Poulos, T. L.; Silverman, R. B. Selective neuronal nitric oxide synthase inhibitors and the prevention of cerebral palsy. *Ann. Neurol.* **2009**, *65*, 209−217.

(20) Kuhn, B.; Gerber, P.; Schulz-Gasch, T.; Stahl, M. Validation and use of the MM-PBSA approach for drug discovery. *J. Med. Chem.* **2005**, *48*, 4040–4048.

(21) Weis, A.; Katebzadeh, K.; Soderhjelm, O.; Nilsson, I.; Ryde, U. Ligand affinities predicted with the MM/PBSA method: Dependence on the simulation method and the force field. *J. Med. Chem.* **2006**, *49*, 6596–6606.

(22) Flinspach, M.; Li, H.; Jamal, J.; Yang, W.; Huang, H.; Silverman, R. B.; Poulos, T. L. Structures of the neuronal and endothelial nitric oxide synthase heme domain with D-nitroarginine-containing dipeptide inhibitors bound. *Biochemistry* **2004**, *43*, 5181–5187.

(23) Li, H.; Shimizu, H.; Flinspach, M.; Jamal, J.; Yang, W.; Xian, M.; Cai, T.; Wen, E. Z.; Jia, Q.; Wang, P. G.; Poulos, T. L. The novel binding mode of *N*-alkyl-*N*′-hydroxyguanidine to neuronal nitric oxide synthase provides mechanistic insights into NO biosynthesis. *Biochemistry* **2002**, *41*, 13868–13875.

(24) Hevel, J. M.; Marletta, M. A. Nitric oxide synthase assays. *Methods Enzymol.* **1994**, *233*, 250–258.

(25) Hah, J. M.; Martasek, P.; Roman, L. J.; Silverman, R. B. Aromatic reduced amide bond peptidomimetics as selective inhibitors of neuronal nitric oxide synthase. *J. Med. Chem.* **2003**, *46*, 1661–1669.

(26) Otwinowski, Z.; Minor, W. Processing of X-ray diffraction data collected in oscillation mode. *Methods Enzymol.* **1997**, *276*, 307–326.

(27) Jones, T. A.; Zou, J.-Y.; Cowan, S. W.; Kjeldgaarrd, M. Improved methods for building models in electron density and the location of errors in these models. *Acta Crystallogr., Sect. A: Found. Crystallogr.* **1991**, *47*, 110–119.

(28) Brunger, A. T.; Adams, P. D.; Clore, G. M.; DeLano, W. L.; Gros, P.; Grosse-Kunstleve, R. W.; Jiang, J.-S.; Kuszewski, J.; Nilges, M.; Pannu, N. S.; Read, R. J.; Rice, L. M.; Simonson, T.; Warren, G. L. Crystallography & NMR System: A new software suite for macromolecular structure determination. *Acta Crystallogr., Sect. D: Biol. Crystallogr.* **1998**, *54*, 905–921.

(29) Massova, I.; Kollman, P. A. Computational alanine scanning to probe protein−protein interactions: A novel approach to evaluate binding free energies. *J. Am. Chem. Soc.* **1999**, *121*, 8133–8143.

(30) Brown, S. P.; Muchmore, S. W. High-throughput calculation of protein-ligand binding affinities: Modification and adaption of the MM-PBSA protocol to enterprise grid computing. *J. Chem. Inf. Model.* **2006**, *46*, 999–1005.

(31) Wang, J.; Wolf, R. M.; Caldwell, J. W.; Kollman, P. A.; Case, D. Development and testing of a general Amber force field. *J. Am. Chem. Soc.* **2004**, *25*, 1157–1174.

(32) Jakalian, A.; Bush, B. L.; Jack, D. B.; Bayly, C. I. Fast, efficient generation of high-quality atom charges. AM1-BCC model: I. Method. *J. Comput. Chem.* **2000**, *21*, 132–146.

(33) Jakalian, A.; Jack, D. B.; Bayly, C. I. Fast, efficient generation of high-quality atom charges. AM1-BCC model: II. Parameterization and validation. *J. Comput. Chem.* **2002**, *23*, 1623–1641.

(34) Harris, D. L.; Park, J. Y.; Gruenke, L.; Waskell, L. Theoretical study of the ligand−CYP2B4 complexes: Effect of structure on binding free energies and heme spin state. *Proteins* **2004**, *15*, 895–914.

JM900007A